Eur. Phys. J. A **27**, XX–XX (2006)
DOI 10.1140/epja/i2005-10264-2

THE EUROPEAN PHYSICAL JOURNAL A

The $K^0_S K^0_S$ final state in two-photon collisions and SU(3) tensor nonets

V.A. Schegelsky, A.V. Sarantsev[a], V.A. Nikonov, and A.V. Anisovich

Petersburg Nuclear Physics Institute, Gatchina, Russia

Received: 25 November 2005 / Revised version: 13 February 2006 /
Published online: 31 March 2006 – © Società Italiana di Fisica / Springer-Verlag 2006
Communicated by A. Schäfer

Abstract. The $K^0_S K^0_S$ final state in two-photon collisions is studied with the L3 experiment at LEP, using orbital angular momentum operators. The mass spectrum is dominated by the formation of tensor mesons, their two-photon partial width are determined. A signal at 1700–1800 MeV is found to be a new tensor state $f_2(1750)$ with mass $M = (1755 \pm 10)$ MeV and width $\Gamma = (67 \pm 12)$ MeV. All observed tensor resonances obey $SU(3)$ relations. The $f_2(1750)$ state forms a second tensor nonet together with $f_2(1560)$ and $a_2(1700)$. The $SU(3)$ analysis allows us to determine with good accuracy mixing angles between nonstrange and strange components of the isoscalar members of tensor nonets.

PACS. 11.80.Et Partial-wave analysis – 13.60.Le Meson production – 13.25.-k Hadronic decays of mesons – 14.40.-n Mesons

1 Introduction

The formation of resonances in two-photon collisions provides a powerful tool for the investigation of meson properties. These data not only supply information about the masses and widths of resonances but also about their couplings to the gamma-gamma channel which can be directly calculated in quark models. Another important feature is that meson molecules and glueball states must be produced weakly in such reactions providing a clear spectrum of quark-antiquark states.

In this paper we study the reaction $e^+e^- \to e^+e^-K^0_S K^0_S$ with an energy-dependent partial wave analysis and discuss the place of the observed states in $SU(3)$ tensor nonets.

Only $J^{PC} = (2n)^{++}$, $n = 0, 1, 2, \ldots$ states decay into two identical neutral pseudoscalar particles. The meson states, consisting of light quarks $n = u$, d and strange quarks s, form meson nonets: three isospin 1, four isospin $\frac{1}{2}$ and two isoscalar states. The isoscalar states can be a mixture of $n\bar{n}$ and $s\bar{s}$ components. The decay of $I = 0$, without strange quarks, and $I = 1$ states into two kaons is defined by the production of an $s\bar{s}$ pair (s-quark exchange) and has the following structure:

$$I = 0: \quad \frac{u\bar{u} + d\bar{d}}{\sqrt{2}} \to K^+K^- + K^0\bar{K}^0,$$
$$I = 1: \quad \frac{u\bar{u} - d\bar{d}}{\sqrt{2}} \to K^+K^- - K^0\bar{K}^0. \qquad (1)$$

If isoscalar and isovector states have similar masses, one observes strong destructive interference in the neutral kaon channel [1]. The $s\bar{s}$ component of $I = 0$ states decays into kaons by u- and d-quark exchange. The calculation of different decay modes from a large set of $I = 0$ states shows that the s-quark exchange is suppressed compared to the nonstrange quark exchange by a factor $\lambda = (0.75–0.85)$. The decay ratios of an observable $I = 0$ state (which can be a mixture of nonstrange and strange components) into different two-body channels are given in table 1, as well as the ratios for an isovector state.

The $e^+e^- \to e^+e^-K^0_S K^0_S$ data used for this analysis correspond to an integrated luminosity of 806 pb^{-1} collected by the L3 detector [2] at LEP around the Z pole (143 pb^{-1}) and at high energies, $\sqrt{s} = 183$–209 GeV (663 pb^{-1}). The $K^0_S K^0_S$ final state in two-photon collisions was studied by L3 [3] and, at lower energies and luminosities, by TASSO, PLUTO and CELLO at PETRA [4].

The EGPC [5] Monte Carlo generator based on the formalism of ref. [6] is used to describe two-photon resonance formation. All generated events passed through the full detector simulation program based on GEANT [7] and GEISHA [8] and reconstructed following the procedure used for the data.

2 Event selection

The selection of $e^+e^- \to e^+e^-K^0_S K^0_S$ events is based on the K^0_S decay into $\pi^+\pi^-$. The events have been col-

[a] e-mail: andsar@pnpi.spb.ru

Table 1. Relation of coupling constants g_a ($a = \pi^0\pi^0$, $\pi^+\pi^-$, $\eta\pi^0$, K^+K^-, $K^0\bar{K}^0$, $\eta\eta$) with nonet coupling g for $q\bar{q}$ mesons decaying into two pseudoscalar mesons in the leading terms of the $1/N$ expansion. Φ is the mixing angle for $n\bar{n} = (u\bar{u} + d\bar{d})/\sqrt{2}$ and $s\bar{s}$ states, and Θ is the mixing angle for η, η' mesons: $\eta = n\bar{n}\cos\Theta - s\bar{s}\sin\Theta$ and $\eta' = n\bar{n}\sin\Theta + s\bar{s}\cos\Theta$. λ is the suppression factor of the s-quark exchange.

Channel	Decay coupling, g_a, for $I = 0$	Decay coupling, g_a, for $I = 1$	Symmetry factor, S_f
$\pi^0\pi^0$	$g\ \cos\Phi/\sqrt{2}$		1/2
$\pi^+\pi^-$	$g\ \cos\Phi/\sqrt{2}$		1
$\eta\pi^0$		$g\ \frac{1}{\sqrt{2}}\cos\Theta$	1
K^+K^-	$g(\sqrt{2}\sin\Phi + \sqrt{\lambda}\cos\Phi)/\sqrt{8}$	$g\sqrt{\lambda}/\sqrt{8}$	1
$K^0\bar{K}^0$	$g(\sqrt{2}\sin\Phi + \sqrt{\lambda}\cos\Phi)/\sqrt{8}$	$-g\sqrt{\lambda}/\sqrt{8}$	1
$\eta\eta$	$g(\cos^2\Theta\ \cos\Phi/\sqrt{2} + \sqrt{\lambda}\ \sin\Phi\ \sin^2\Theta)$		1/2

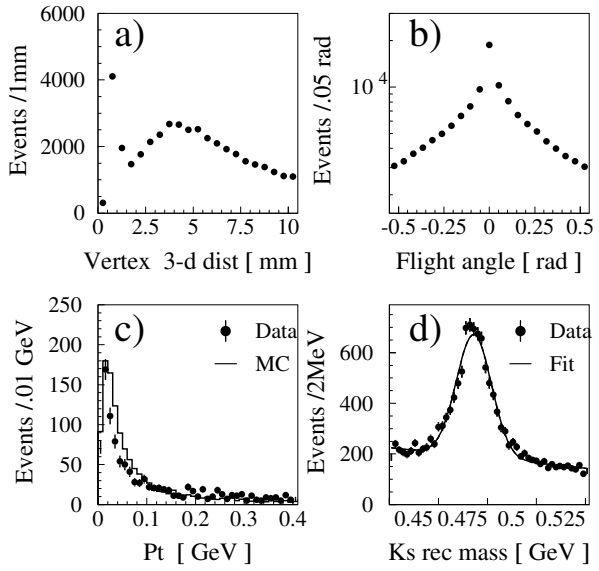

Fig. 1. a) Invariant 3-dimensional distance between the primary and the secondary vertex; b) the angle in the transverse plane between the flight direction and the total momentum for the K^0_S candidates; c) the total transverse momentum imbalance; d) the $\pi^+\pi^-$ mass spectrum for reconstructed secondary vertices.

lected predominantly using the charged-particle track triggers [9], exploiting the central tracking system. To veto π^0's and photons the electromagnetic calorimeter is also used in the selection.

The following criteria are used:

- There must be exactly four charged tracks in the tracking system with a net charge of zero; not more than 2 tracks should originate from the primary vertex within 3 standard deviations.
- Events with photons are rejected. A photon is identified as an isolated shower, with more than one crystal in the electromagnetic calorimeter, with at least 100 MeV energy. The isolation cut requires no corresponding track inside a cone of 0.2 rad.

The K^0_S are identified by the secondary vertex reconstruction.

- A secondary vertex should have an "invariant" distance d greater than 1.5 mm

$$d = d_0 \frac{M_{Ks}}{P_{Ks}}, \tag{2}$$

  where d_0 is the distance in space between the primary and secondary vertex (fig. 1a).
- To eliminate the secondary vertex from $\gamma \to e^+e^-$ conversions, the cosine of the angle between π^+ and π^- should be less than 0.95.
- The angle α between the flight direction of the K^0_S candidate, taken as a line between the interaction point and the secondary vertex in the transverse plane, and the total transverse momentum vector of the decay pions must be smaller than 0.3 rad (fig. 1b).
- The total transverse momentum imbalance $P_t = |\sum \mathbf{p}_t|$ must be smaller than 0.3 GeV. In fig. 1c the P_t distribution is compared to the Monte Carlo prediction for exclusive $K^0_S K^0_S$ formation. The excess of the data at high values of P_t is due to $K^0_S K^0_S$ events with missing particles.

The $\pi^+\pi^-$ mass distribution is shown in fig. 1d, a mass resolution $\sigma = 9.5 \pm 0.2$ MeV is observed. Figure 2 shows the distribution of the mass of one K^0_S candidate *vs.* the mass of the other candidate. There is a strong enhancement corresponding to the $K^0_S K^0_S$ formation. We require that the reconstructed masses of two K^0_S candidates must be inside a circle of 40 MeV radius centered on the peak of the $K^0_S K^0_S$ signal. Events inside a ring of the same surface outside of the circle are used as an estimate of the background in the accepted events sample.

With these selection criteria 870 events are found. The background due to misidentified K^0_S pairs is estimated to be less than 10%.

Figure 3 shows the $K^0_S K^0_S$ mass spectrum of selected events with the mass spectrum of the background estimated as mentioned above.

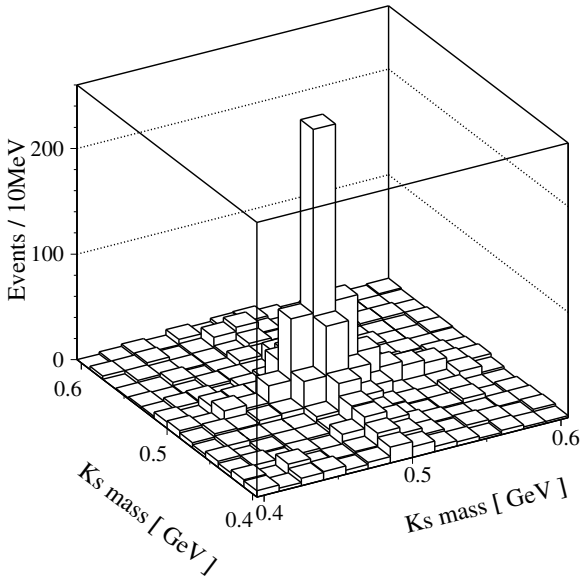

Fig. 2. The distribution of the mass of one K^0_S candidate *vs.* the mass of the other candidate.

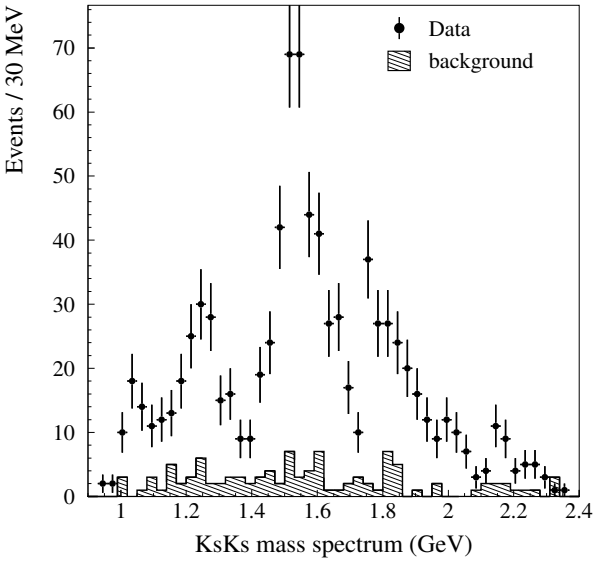

Fig. 3. The $K^0_S K^0_S$ mass spectrum of selected events with the mass spectrum of the background.

3 Partial wave analysis

In the present analysis, resonances are parameterised as Breit-Wigner amplitudes with corresponding energy space factors and standard Blatt-Weisskopf factors $F(r,k,L)$ [10] calculated with an interaction radius $r = 0.55\,\mathrm{fm}$:

$$A^S = \frac{g^S_{\gamma\gamma} g_{KK}}{M^2 - s - iM\Gamma}\ \frac{1}{\sqrt{2}} \times \frac{|\mathbf{k}_{\gamma\gamma}|^{L_{\gamma\gamma}}\ |\mathbf{k}_{KK}|^{L_{KK}} \mathcal{F}^J_S(\cos\Theta)}{\sqrt{F(r,k_{\gamma\gamma},L_{\gamma\gamma})F(r,k_{KK},L_{KK})}}, \qquad (3)$$

where S is the total spin of two photons, J is the resonance spin, $g^S_{\gamma\gamma}$ and g_{KK} are the production and decay couplings, respectively, $k_{\gamma\gamma}$ and k_{KK} the momenta, defined in the center of mass of the resonance, $L_{\gamma\gamma}$ and L_{KK} are the orbital angular momenta of the production and decay system. The correct phase space factor for production and decay channels as well as the angular dependence is provided by orbital angular momentum operators in the numerator. Due to the spinless nature of the final state particles the amplitude structure for the decay of resonances into $K^0_S K^0_S$ is defined by orbital angular momentum operators only. These operators are constructed with the kaons momenta [11].

Two quasi-real photons with orbital angular momentum L and total spin S ($S = 0, 2$) form resonances with spin J corresponding to a $^{2s+1}L_J$ two-photon state. A 0^{++} state is produced by only the $^1S_0$ combination of spin and orbital angular momentum operators, while the 2^{++} partial wave can be produced from a spin-0 state with $L = 2$ ($^1D_2$) or from a spin-2 state with $L = 0$ ($^5S_2$). For a 4^{++} state there are also two possible combinations: $^1G_4$ and $^5D_4$. The form of the $\gamma\gamma$ operators used in the present calculations was taken from [12]. The product of operators for $\gamma\gamma$ and KK channels leads to the following angular dependencies for partial wave amplitudes:

$$^5(L_{\gamma\gamma})_J \to ^5\,(L_{KK})_J:\ \mathcal{F}^J_2(\cos\Theta) = \frac{P''_J(\cos\Theta)}{(J-1)J}\sin^2\Theta,$$
$$^1(L_{\gamma\gamma})_J \to ^1\,(L_{KK})_J:\ \mathcal{F}^J_0(\cos\Theta) = P_J(\cos\Theta). \qquad (4)$$

Here $L_{KK} = J$ and $L_{\gamma\gamma} = J - S$. The polarization of the initial photons is not measured and states with different spin do not interfere in the reaction. Thus the amplitude for scalar states $^1S_0$ might interfere only with $^1D_2$ and $^1G_4$ amplitudes. The $^5S_2$ amplitude, which is the strongest in the data, interferes only with the 4^{++} $^5D_4$ partial wave.

The mass distribution from $\gamma\gamma \to K^0_S K^0_S$ reaction is shown in fig. 3 and the angular distribution for the total mass region in fig. 4a. It is seen that the angular distribution follows a $\sin^2\Theta$ shape. However, our acceptance falls rapidly for small $\sin\Theta$, and it is not easy to distinguish between production of tensor and scalar states.

The $K^0_S K^0_S$ mass spectrum exhibits a clear resonance structure. Despite their large two-photon widths, the $f_2(1270)$ and the $a_2(1320)$ resonances produce a small signal due to destructive interference [1]. The spectrum is dominated by the formation of $f'_2(1525)$. Close to the $K\bar{K}$ threshold, the signal from the $a_0(980)$ and/or $f_0(980)$ state is also seen.

The coupling for the first tensor nonet is calculated from the $K\bar{K}$ width of $f'_2(1525)$: $65 \pm 5\,\mathrm{MeV}$ [13]. The relation between nonet coupling and partial widths is defined as

$$\frac{g_a^2\ S_f\ k_M^{2L}\rho(M^2)}{F(r,k_M,L)} = M\Gamma\,,$$
$$\rho(s) = \sqrt{\frac{s-4m_K^2}{s}}\,, \qquad (5)$$

where S_f is isotopic coefficient given in table 1, k is the relative momentum of kaons and $L \equiv L_{KK}$ is the orbital

Table 2. Coupling constants, mixing angles and decay widths for tensor nonets calculated from the $SU(3)$ fit. Values with asterisk were fixed from other results [13,14].

	First nonet			Second nonet		
	$a_2(1320)$	$f_2(1270)$	$f_2'(1525)$	$a_2(1700)$	$f_2(1560)$	$f_2(1750)$
Mass (MeV)	1304 ± 10	1277 ± 6	1523 ± 5	1730^*	1570^*	1755 ± 10
Width (MeV)	120 ± 15	195 ± 15	104 ± 10	340^*	160^*	67 ± 12
$K\bar{K}$ width (MeV)	$7.0^{+2.0}_{-1.5}$	7.5 ± 2	68^*	5 ± 3	2 ± 1	17 ± 5
Nonet coupling (MeV)	0.95 ± 0.08			0.35 ± 0.05		
$SU(3)$ violation factor	0.85 ± 0.1	0.95 ± 0.1	1.1 ± 0.1	1.0^*		
Mixing angle (degrees)	-1 ± 3			-10^{+5}_{-10}		
$\gamma\gamma$ width (keV)	0.91^*	2.55 ± 0.15	0.13 ± 0.03	0.30 ± 0.05	0.70 ± 0.14	0.13 ± 0.04
$\pi\pi$ width (MeV)		152 ± 8	$0.2^{+1.0}_{-0.2}$		25^*	1.3 ± 1.0
$\pi\eta$ width (MeV)	18.5 ± 3			9.5 ± 2		
$\eta\eta$ width (MeV)		1.8 ± 0.4	5.0 ± 0.8		1.2 ± 0.3	2.0 ± 0.5

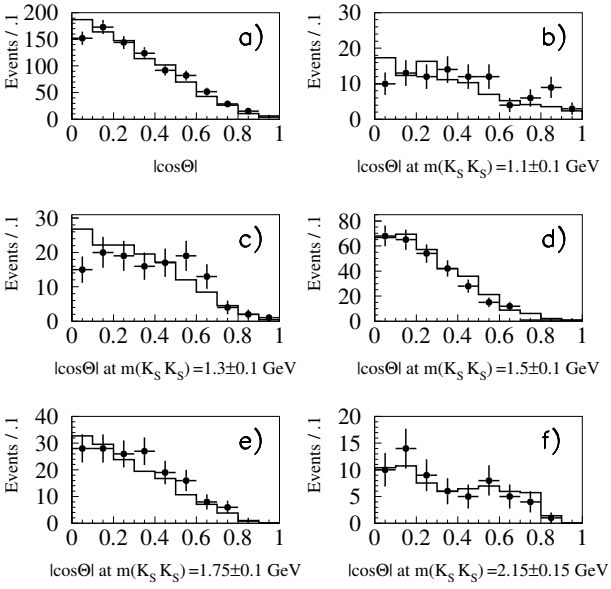

Fig. 4. The angular distributions on $\gamma\gamma \to K^0_S K^0_S$ reaction. The data corresponds to points with error bars, the description of the data (for the fit with nonet relations imposed) is shown by solid curves.

moment of the decay of a reasonance with mass M. Assuming that this resonance is a pure $s\bar{s}$ state we obtain $g = 0.96 \pm 0.08\,\mathrm{GeV}$. This value reproduces $\eta\eta$ width of $f_2'(1525)$ as well as $\pi\pi$, $K\bar{K}$ and $\eta\eta$ widths of $f_2(1270)$ (see table 2) within errors given in PDG [13]. However, the calculated $\pi\eta$ and $K\bar{K}$ widths for $a_2(1320)$ appear to be about 20% higher than PDG value, which provides us a scale for $SU(3)$ violation in this nonet. These $SU(3)$ violation factors are introduced in the fit to obtain the better agreement with present experimental data as well as with branching ratios of the resonances.

$SU(3)$ imposes strong relations between the $\gamma\gamma$ widths of the nonet members. Here the $\gamma\gamma$ coupling is defined by the charge factors and related as $1/\frac{5}{\sqrt{2}}/\frac{3}{\sqrt{2}}$ for $s\bar{s}$, $(u\bar{u}+d\bar{d})/\sqrt{2}$ and $(u\bar{u}-d\bar{d})/\sqrt{2}$ components. For example, the ratio of pure isoscalar and isovector states is 25/9, which is in perfect agreement with the measured values for $f_2(1275)$ and $a_2(1320)$.

For the isoscalar S-wave resonances we use the P-vector approach with K-matrix parameterisation taken from [15] and impose $SU(3)$ relations. There are no free parameters in this amplitude for the resonance part. The $\gamma\gamma$ couplings are also determined from $SU(3)$ apart from overall scale.

A contribution from 4^{++} state might be seen from the angular distributions at higher invariant masses in fig. 4. The mass and the width and the $\Gamma_{\gamma\gamma}$-coupling of this state are the parameters. From the fit we obtain a resonant contribution with mass of $2150 \pm 30\,\mathrm{MeV}$ and width of $50 \pm 20\,\mathrm{MeV}$. It can be a real signal from a dominantly $s\bar{s}$ 4^{++} state which was not observed before. However, on

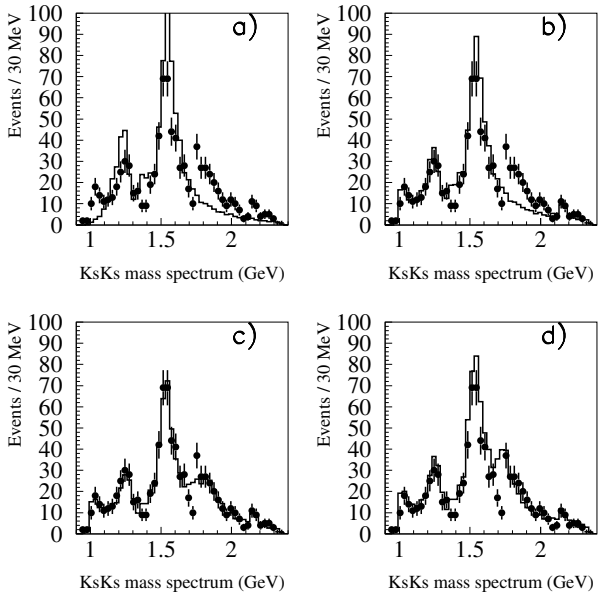

Fig. 5. a) The description of the data with the first tensor nonet states only. b) Description of the data with the first tensor nonet, scalar states and a 4^{++} resonance. c) Fit of the data with components described in b) and the $f_0(1710)$ state fitted with free parameters. d) Same as c) but mass and width of $f_0(1710)$ are fixed from latest BES results [16].

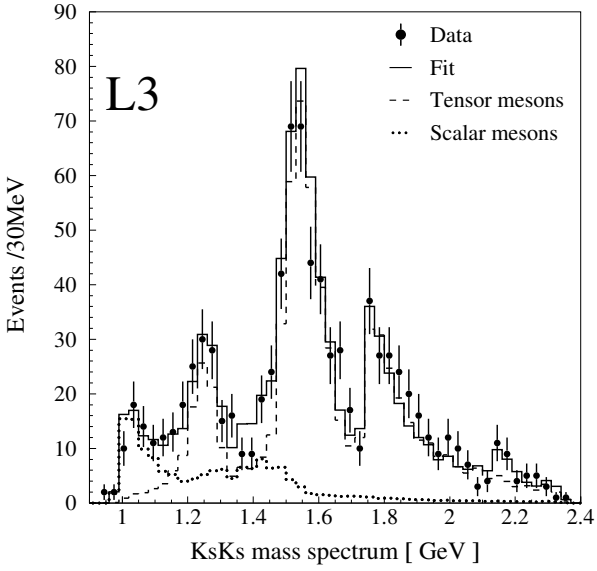

Fig. 6. The description of the $\gamma\gamma$ spectrum. The data are shown as points with error bars, the solid curve corresponds to the fit with nonet relations imposed, the dashed line shows the contribution of tensor states and the dotted line the contribution of scalar states.

the basis of the present statistics (the significance is only 2σ), we cannot exclude a statistical fluctuation.

In the fit we introduced coherent nonresonant contributions in all partial waves. These contributions were found to be small but useful to reproduce the $K^0_S K^0_S$ spectrum in the nonresonant region.

The description of the data with these components is shown in fig. 5a, b. The fit reproduces reasonably well the mass region below 1650 MeV and above 1900 MeV, but clearly failes to describe the 1700–1800 MeV mass region.

By introducing an additional tensor resonance with 1755 ± 10 MeV mass and full width 67 ± 12 MeV, we find a good description of the mass spectrum (fig. 6). The fit describes well the dip in the region 1.7 GeV by a destructive interference between $f'_2(1525)$ and $f_2(1750)$ states. If a scalar f_0 state is introduced instead of $f_2(1750)$, the mass of this scalar is found to be 1805 ± 30 MeV and the width 260 ± 30 MeV, but the fit fails to reproduce the dip at 1700 MeV and the slope above 1800 MeV, as shown in fig. 5b. A f_0 state can only interfere with the $^1D_2$ component naturally whuch is much weaker than the $^5S_2$ wave. The $^1D_2$ contribution can be easily defined from the angular distribution and is found to be very small compared to the $^5S_2$-wave. This phenomenon was observed in $\gamma\gamma$ production of tensor states into other final states [17,18] and explained from the calculation of quark diagrams [12]. Therefore the f_0 and f_2 contributions interfere only very weakly and their cross-sections are added, filling the dip at 1700 MeV. In contrast, the $f_2(1750)$ resonance interferes with the tail of the $f'_2(1525)$ producing a dip.

4 SU(3) tensor nonets

We have fitted the $I = 0$ and $I = 1$ states belonged to the first and second radial $SU(3)$ tensor nonets, using parameters for the $a_2(1320)$ and $a_2(1700)$ states found with the L3 experiment [17] and defining parameters for the $f'_2(1525)$ and $f_2(1750)$ states from the present analysis. The ratios for the production of tensors from $^1D_2$ and $^5S_2$ $\gamma\gamma$ channels were first fitted; the result agrees with values calculated in [12]. So in the final fit these ratios were fixed at the predicted values.

With $SU(3)$ relations imposed, the only parameters to fit the data are masses, widths, the nonet mixing angles and $SU(3)$ violation factors.

We find very good description of the data as presented in fig. 6. The quality of this fit is similar to the one obtained with the energy-dependent partial wave analysis without imposing nonet classification. The masses, widths, $K\bar{K}$ couplings, mixing angles and partial widths of the states are given in table 2. Moreover, if the $SU(3)$ constrain is taken out the parameters do not move from $SU(3)$ values for more than 20%.

The $f_2(1560)$ and $a_2(1700)$ states give very small contribution to the $K^0_S K^0_S$ cross-section. This is not a surprise: these states have small branching for decay into two pseudoscalars and a radial excitation they also have small $\gamma\gamma$ widths of states. The partial width of the $f_2(1560)$ state was estimated in [14] to be less than 25 MeV. To derive a branching ratio for $f_2(1560) \to K\bar{K}$, we fixed the $\gamma\gamma$ width to 25 MeV. Of course, a smaller $\gamma\gamma$ width would result in a large $K\bar{K}$ width. The corresponding values for the $K\bar{K}$ partial widths are given in table 2 and show very small

contributions of these states to the reaction considered. This is not the case for $f_2(1750)$, where $SU(3)$ calculation gives a reasonably large $K\bar{K}$ branching ratio and due to a narrow total width we obtain a large branching ratio into the two-kaon channel.

The mixing angle of the first tensor nonet was found to be close to zero: (-1 ± 3) degrees. The fit is very sensitive to this value. Already at two standard deviations the problems in the description of $K^0_S K^0_S$ spectrum are clearly visible. The mixing angle of the second nonet is found to be -10^{+5}_{-10} degrees.

A description of the data within of $SU(3)$ nonets has a significant problem if the peak at 1750 MeV is assumed to be a scalar state [13]. If this state is a nonet partner of one of the known states, $f_0(1370)$ or $f_0(1500)$, then the calculated signal is too weak to fit the data. If the $K\bar{K}$ coupling of this scalar state is left free in the fit, we find that it must be about 4 times bigger than the total width of the resonance, due to the small factor and the absence of interference with the $f_2'(1525)$ tail.

5 Summary

We have performed a study of $\gamma\gamma$ fusion into $K^0_S K^0_S$ data. The reaction is dominated by production of tensor mesons. In addition to the well known $f_2(1275)$, $a_2(1720)$ and $f_2(1525)$ we found evidence for a further tensor state with mass 1755 ± 10 MeV and width 67 ± 12 MeV. Although a scalar state is not forbidden by angular distributions, it fails to describe simultaneously the dip at 1700 MeV and the slope at masses higher than 1750 MeV. When $SU(3)$ nonet relations are applied, this state is revealed as a solid member of the second tensor nonet together with $f_2(1560)$ and $a_2(1700)$ states. The mixing angles are determined to (-1 ± 3) degrees for the first and (-10^{+5}_{-10}) for the second tensor nonet.

We are very grateful to V.V. Anisovich and E. Klempt for extremely useful discussions and comments. V.A. Schegelsky thanks members of L3 Collaboration, especially S.C.C. Ting, for constructive discussions. This work was partly supported by the Russian Foundation for Basic Research (grant 04-02-17091).

References

1. H.J. Lipkin, Nucl. Phys. B **7**, 321 (1968); D. Faiman *et al.*, Phys. Lett. B **59**, 269 (1975).
2. L3 Collaboration (B. Adeva *et al.*), Nucl. Instrum. Methods A **289**, 35 (1990); L3 Collaboration (O. Adriani *et al.*), Phys. Rep. **236**, 1 (1993); M. Chemarin *et al.*, Nucl. Instrum. Methods A **349**, 345 (1994); M. Acciarri *et al.*, Nucl. Instrum. Methods A **351**, 300 (1994); I.C. Brock *et al.*, Nucl. Instrum. Methods A **381**, 236 (1996); A. Adam *et al.*, Nucl. Instrum. Methods A **383**, 342 (1996).
3. L3 Collaboration (M. Acciarri *et al.*), Phys. Lett. B **363**, 118 (1995); L3 Collaboration (M. Acciarri *et al.*), Phys. Lett. B **501**, 173 (2001);
4. TASSO Collaboration (M. Althoff *et al.*), Phys. Lett. B **121**, 216 (1982); TASSO Collaboration (M. Althoff *et al.*), Z. Phys. C **29**, 189 (1985); PLUTO Collaboration (C. Berger *et al.*), Z. Phys. C **37**, 329 (1988); CELLO Collaboration (H.J. Behrend *et al.*), Z. Phys. C **43**, 91 (1989).
5. F.L. Linde, *Charm Production in Two-Photon Collisions*, PhD Thesis, Rijksuniversiteit, Leiden (1988).
6. V.M. Budnev *et al.*, Phys. Rep. C **15**, 181 (1975).
7. R. Brun *et al.*, GEANT 3.15 preprint CERN DD/EE/84-1 (1984); revised, 1987.
8. H. Fesefeldt, RWTH Aachen report PITHA 85/2 (1985).
9. P. Béné *et al.*, Nucl. Instrum. Methods A **306**, 150 (1991); D. Haas *et al.*, Nucl. Instrum. Methods A **420**, 101 (1999).
10. F. Von Hippel, C. Quigg, Phys. Rev. D **5**, 624 (1972).
11. A.V. Anisovich, V.V. Anisovich, V.N. Markov, M.A. Matveev, A.V. Sarantsev, J. Phys. G **28**, 15 (2002).
12. A.V. Anisovich, V.V. Anisovich, M.A. Matveev, V.A. Nikonov, Phys. At. Nucl. **66**, 914 (2003).
13. Particle Data Group (K. Hagiwara *et al.*), Phys. Rev. D **66**, 1 (2002).
14. Crystal Barrel Collaboration (V.V. Anisovich *et al.*), Phys. Lett. B **323**, 233 (1994); C.A. Baker *et al.*, Phys. Lett. B **467**, 147 (1999).
15. V.V. Anisovich, A.V. Sarantsev, Eur. Phys. J. A **16**, 229 (2003).
16. BES Collaboration (J.Z. Bai *et al.*), Phys. Lett. B **472**, 207 (2000).
17. V.A. Schegelsky *et al.*, *Partial wave analysis of* $\pi^+\pi^-\pi^0$ *production in two-photon collisions at LEP*, this issue.
18. H. Albrecht *et al.*, Z. Phys. C **74**, 469 (1997); ARGUS Collaboration (H. Albrecht *et al.*), Z. Phys. C **50**, 1 (1991).